Adsorption, 1, 291–301 (1995)

Effect of Pore Size Distribution on the Surface Diffusivity in Activated Carbon: Hybrid Dubinin-Langmuir Isotherm

H.D. DO AND D.D. DO
Department of Chemical Engineering, University of Queensland, Brisbane, QLD 4072, Australia

Received August 18, 1994; Revised March 31, 1995; Accepted May 4, 1995

Abstract. The concentration dependence of the observed surface diffusivity for activated carbon due to the pore size distribution is theoretically investigated. The mathematical model is derived based on the assumption of a local hybrid adsorption isotherm (proposed recently by Shethna and Bhatia, 1994) and a local surface diffusive flux for a particular pore of half width r. Using those local quantities and assuming a Gamma pore size distribution, the observed surface diffusivity is obtained. This observed surface diffusivity was found to increase rapidly with loading if the chemical potential is the driving force for surface flow. Furthermore, this observed surface diffusivity, $D/D(0)$, was found to be the same as the Darken thermodynamic correction factor, using only the macroscopic isotherm information. This indicates that the thermodynamic correction factor contains information on the averaging of the surface heterogeneity.

Keywords: hybrid isotherm, darken, surface diffusivity

1 Introduction

The effects of micropore size distribution on the variation of the surface diffusivity with loading in microporous solids are studied previously by Do and Do (1993). The observed surface diffusivity was found to be very sensitive to the mean pore size and pore variance, suggesting the structure heterogeneity is one possible source responsible for the observed surface diffusivity to increase with loading. The overall adsorption isotherm was obtained by averaging the local isotherm over the micropore size distribution, and the form of this local isotherm was assumed the same irrespective of the pore size, implying that the mechanism of adsorption is the same in all pores. This is a somewhat ideal assumption as one would expect the adsorption mechanism would vary from pores of molecular dimension to pores of macro-dimension. This should be expected in many solids, at least in the case of activated carbon where the pore size distribution is very broad.

For small pores, i.e. micropores, the appropriate mechanism for such pores is the pore filling mechanism (Gregg and Sing, 1982; Rudzinski and Everett, 1992) and hence the local isotherm of the form Dubinin-Radushkevich (1947) equation or its varieties is the appropriate choice. However the DR equation does not exhibit proper Henry limit at zero pressure. The Langmuir equation is frequently used in the literature to describe adsorption in small pores as well as large pores. Although it is physically incorrect to use the Langmuir equation to describe adsorption in micro pore range because it was derived based on the site-adsorption assumption, Bhatia and Shethna (1994) proposed a method by combining the Henry law feature of the Langmuir equation to the Dubinin equation. The hybrid isotherm of Bhatia and Shethna is valid over the whole pressure range (i.e eliminating the non Henry's law behaviour of DR equation) and is applicable for all pores. The purpose of this work is to apply the concept of hybrid isotherm to study the concentration dependence of the observed surface diffusivity due to the pore size distribution.

2 Model Development

2.1 Hybrid Adsorption Model for Micropores

The adsorption equilibrium between a gas of pressure P and an adsorbed phase in a pore having a half width r is considered to follow a hybrid local isotherm. This isotherm is taken to be described by the Dubinin-Astakhov equation (1971) if the pressure is above a

threshold pressure $P_t(r, T)$, which is a function of the pore half width and temperature. Below this threshold pressure, the isotherm is assumed to follow a Langmuir equation. The hybrid isotherm is:

$$\theta(r, P, T) = \begin{cases} \theta_L(r, P, T), & P \le P_t(r, T) \\ \theta_D(r, P, T), & P \ge P_t(r, T) \end{cases} \quad (1)$$

where the Langmuir and Dubinin fractional loadings are given by:

$$\theta_L(r, P, T) = \frac{K(r, T)(P/P^0)}{1 + K(r, T)(P/P^0)};$$
$$\theta_D(r, P, T) = \exp\left(-\left\{\frac{RT}{\beta E_0}\ln\left(\frac{P^0}{P}\right)\right\}^n\right) \quad (2)$$

The characteristic energy $E_0(r)$ is assumed to take the form, $E_0(r) = k/r$, where $k = 12$ kJ.nm/mole for slit-like pores. Other forms available in the literature can be equally applied.

What need to be obtained in Eq. (1) are the Langmuir affinity constant and the threshold pressure. They are found by simply matching the fractional loadings and their slopes of the two mechanisms at the threshold pressure (Shethna and Bhatia, 1994). By so doing, we obtain:

$$K = Q\exp\left[n(1+Q)\ln\left(\frac{1+Q}{Q}\right)\right];$$
$$P_t = \frac{P^0}{\exp\left(n(1+Q)\ln\left(\frac{1+Q}{Q}\right)\right)} \quad (3)$$

where $Q(r, T)$ is the solution of the following non linear algebraic equation

$$(1+Q)^{n/(n-1)}\ln\left(\frac{1+Q}{Q}\right) = \left[\frac{\beta E_0(r)}{nRT}\right]^{n/(n-1)} \quad (4)$$

Thus, for a given set of E_0, β, n and T, Eq. (4) can be solved for Q, and then the Langmuir affinity constant and the threshold pressure are obtained from Eq. (3). For a given pore of half width r, the nonlinear equation for Q may yield two solutions. The physically acceptable solution is the one that shows an increase in Q with decreasing r. The behaviour of $Q(r, T)$ at small pore half width r obtained from Eq. (4) by taking its limit when $r \to 0$

$$\lim_{r\to 0} Q = \exp\left[-\left(\frac{\beta E_0}{nRT}\right)^{n/(n-1)}\right] \to 0 \quad (5)$$

and the behaviour of the Langmuir affinity constant is then:

$$\lim_{r\to 0} K = \lim_{r\to 0}\frac{[(1+Q)/Q]^n}{1/Q} = \begin{cases} 0 & \text{for } n < 1 \\ 1 & \text{for } n = 1 \\ \infty & \text{for } n > 1 \end{cases} \quad (6)$$

The above equations show that $K(r, T)$ decreases with decreasing n. It is physically expected that the adsorption affinity is large in small pores due to their restricted environment. Therefore, the acceptable value for n should be greater than unity ($n > 1$).

For a given pressure P, there exists a threshold pore half width, r_t, such that for pores having half width less than r_t, the Dubinin pore filling mechanism is operative while the Langmuir mechanism is functioning in pores having half width greater than r_t. The threshold pore half width is:

$$r_t = \frac{\beta k}{RT}\frac{1}{\left\{n(1+Q_t)\left[\ln\left(\frac{P^0}{P}\right)\right]^{n-1}\right\}^{1/n}},$$
$$P = \frac{P^0}{\exp\left(n(1+Q_t)\ln\left(\frac{1+Q_t}{Q_t}\right)\right)} \quad (7)$$

Equation (7) suggests that as P increases the threshold half width also increases, that is more pores are filled with adsorbate (Dubinin mechanism). Physically, there must be constraint on this threshold half width because the pore filling mechanism can not occur in pores having size in the range of mesopore or macropore. The maximum threshold half width above which the Dubinin mechanism ceases to operate can also be obtained from Eq. (4), when the solution for Q is a double root, that is:

$$r_m = \frac{\beta k}{RT}\frac{1}{n(1+Q_m)\left[\ln\left(\frac{1+Q_m}{Q_m}\right)\right]^{(n-1)/n}},$$
$$Q_m\ln\left(\frac{1+Q_m}{Q_m}\right) = \frac{n-1}{n} \quad (8)$$

The Langmuir affinity and the threshold pressure corresponding to this maximum threshold half width, respectively, are:

$$K_m = Q_m\exp\left[n(1+Q_m)\ln\left(\frac{1+Q_m}{Q_m}\right)\right];$$
$$P_m = \frac{P^0}{\exp\left(n(1+Q_m)\ln\left(\frac{1+Q_m}{Q_m}\right)\right)} \quad (9)$$

The range of micropore size over which the volume filling mechanism is operative is between r_0 and r_m,

where r_0 is the minimum pore half width of the solid structure. The maximum threshold pore size, r_m, can be regarded as the demarcation half width separating micropore and mesopore.

2.2 *Surface Adsorption for Macropores*

We have obtained the necessary equations for micropores and the important results are the threshold pore size, r_t, at a given pressure and the demarcation pore size, r_m, separating the micropore range from the mesopore range. For pores having size larger than r_m, it is reasonable to assume that the mechanism of adsorption is that by surface layering, that is:

$$\theta_S = \frac{c(P/P^0)}{1+(c-1)(P/P^0)} \tag{10}$$

where c is the affinity parameter of the surface adsorption. At the transition point between micropore and mesopore ($r = r_m$), the Langmuir equation used for micropore (Eq. 2) should match the macropore surface adsorption term (Eq. 10). This suggests that the affinity constant c in Eq. (10) is equal to K of Eq. (2) evaluated at $r = r_m$, that is:

$$c \cong K_m = K(r_m, T) \tag{11}$$

2.3 *Overall Adsorption*

Knowing the appropriate adsorption equations in each pore range, the observed adsorbed concentration is simply the integration of the local isotherm over the pore size distribution $F(r)$

$$C(P,T) = \frac{V}{v_M}\int_{r_0}^{r_t(P)} \theta_D F(r)dr + \frac{V}{v_M} \times \int_{r_t(P)}^{r_m} \theta_L F(r)dr + \frac{2V}{A}\int_{r_m}^{\infty} \theta_S \frac{F(r)}{r}dr \tag{12}$$

where θ_D, θ_L are given in Eq. (2), and θ_S is given in Eq. (10). Here V is the total pore volume, μ_M is the liquid molar volume, and A is the adsorbate molar area. The first integral of the hybrid isotherm represents pore filling by Dubinin mechanism which is valid in pores having size from r_0 to the threshold pore size $r_t(P)$, the second integral is the Langmuir sorption in micropores prevailed in pores having size from $r_t(P)$ to the demarcation pore size r_m. Finally, third integral is the surface adsorption for mesopore and macropore.

To perform later computation, we assume the pore size distribution takes the form of gamma distribution (Jaroniac and Madey, 1988).

$$F(r) = \frac{2q^{m+1}}{\Gamma(m+1)}(r-r_0)^{2m+1}\exp[-q(r-r_0)^2] \quad \text{for } r > r_0 \tag{13}$$

The overall fractional loading can be obtained from Eq. (12):

$$\theta_{\text{obs}} = S_1\int_{r_0}^{r_t(P)} \theta_D F(r)dr + S_1\int_{r_t(P)}^{r_m} \theta_L F(r)dr + S_2\int_{r_m}^{\infty} \theta_S \frac{F(r)}{r}dr \tag{14}$$

where S_1 and S_2 are defined as follows

$$S_1 = \frac{V}{v_M}\left(\frac{1}{C_{\max}}\right), \quad S_2 = \frac{2V}{A}\left(\frac{1}{C_{\max}}\right);$$
$$C_{\max} = \frac{V}{v_M}\int_{r_0}^{r_m} F(r)dr + \frac{2V}{A}\int_{r_m}^{\infty}\frac{F(r)}{r}dr \tag{15}$$

Equation (14) is our desired equation for the calculation of the overall fractional loading.

2.4 *Surface Flux*

2.4.1 Concentration Gradient as Driving Force. If the concentration gradient is assumed as the driving force for the transport of the adsorbed species. The local flux of the adsorbed species is assumed to be proportional to the local adsorbed concentration gradient

$$J = -D_s(r)\cdot C_{\max}\frac{d\theta(x,r,P,T)}{dx};$$
$$D_s(r) = D_{s0}\exp\left(-a\frac{\alpha}{r}\right) \tag{16}$$

where $D_s(r)$ is the local surface diffusivity at the pore level. Assumed a patchwise topography, the observed flux can be obtained by integrating the local flux over the pore volume distribution:

$$J_{\text{obs}} = C_{\max}\int_{r_0}^{\infty} D_s(r)\frac{d\theta}{dx}F(r)dr \tag{17}$$

This observed flux is obtained from the information of microscopic fluxes at pore level. If we define the macroscopic surface diffusivity as:

$$J_{\text{obs}} = -D_{\text{obs}}C_{\max}\frac{d\theta_{\text{obs}}}{dx} \tag{18}$$

where D_{obs} is the macroscopic surface diffusivity, and θ_{obs} is the macroscopic fractional loading. Equating Eqs. (17) and (18) and using Eq. (14), and integrating the resulting over a particle of length L, we obtain after following the procedure of Do and Do (1993):

$$\frac{D_{obs}}{D_{s0}} = \frac{\langle\theta_D\rangle_2 + \langle\theta_L\rangle_2 + \langle\theta_S\rangle_2}{\langle\theta_D\rangle_1 + \langle\theta_L\rangle_1 + \langle\theta_S\rangle_1} \tag{19}$$

where the quantities in the RHS are given in the appendix for the case of $n = 2$ (DR).

2.4.2 Chemical Potential as Driving Force. When the driving force for the surface flow is due to the chemical potential gradient rather than the concentration gradient, the flux of adsorbed species is

$$J(x;r) = -D_s(r) \cdot C_{max} \frac{\theta}{P} \frac{dP}{d\theta} \frac{d\theta}{dx} \tag{20}$$

Follows the same procedure described above, we obtain the following expression for the observed surface diffusivity

$$\frac{D_{obs}}{D_{s0}} = \frac{\langle\theta_D\rangle_3 + \langle\theta_L\rangle_3 + \langle\theta_S\rangle_3}{\langle\theta_D\rangle_1 + \langle\theta_L\rangle_1 + \langle\theta_S\rangle_1} \tag{21}$$

The definitions of all terms in the RHS are given in the appendix. The difference between Eqs. (19) and (21) is the definition of the numerator.

2.4.3 Darken Relation. The observed surface diffusivity calculated as in Eq. (21) is compared with the diffusivity calculated based on the thermodynamic correction factor, given below:

$$\frac{D}{D_{s0}} = \frac{d\ln P}{d\ln C} \quad \text{or} \quad \frac{D}{D_{s0}} = \left(\frac{C}{P}\right)\left(\frac{dC}{dP}\right)^{-1} \tag{22}$$

The derivative dC/dP is obtained by taking differentiation of the adsorbed concentration $C(P, T)$ of Eq. (12) with respect to P.

3 Results and Discussion

3.1 Mechanism of Adsorption in Micropores

The essential features of the hybrid isotherm are illustrated in Fig. 1. When the gas pressure is less than the threshold pressure P_ε, corresponding to the smallest pore size r_0, Langmuir sorption is the only mechanism operating in all micropores, and surface adsorption mechanism is operative in the macropore range (Fig. 1a). When the gas phase pressure exceeds

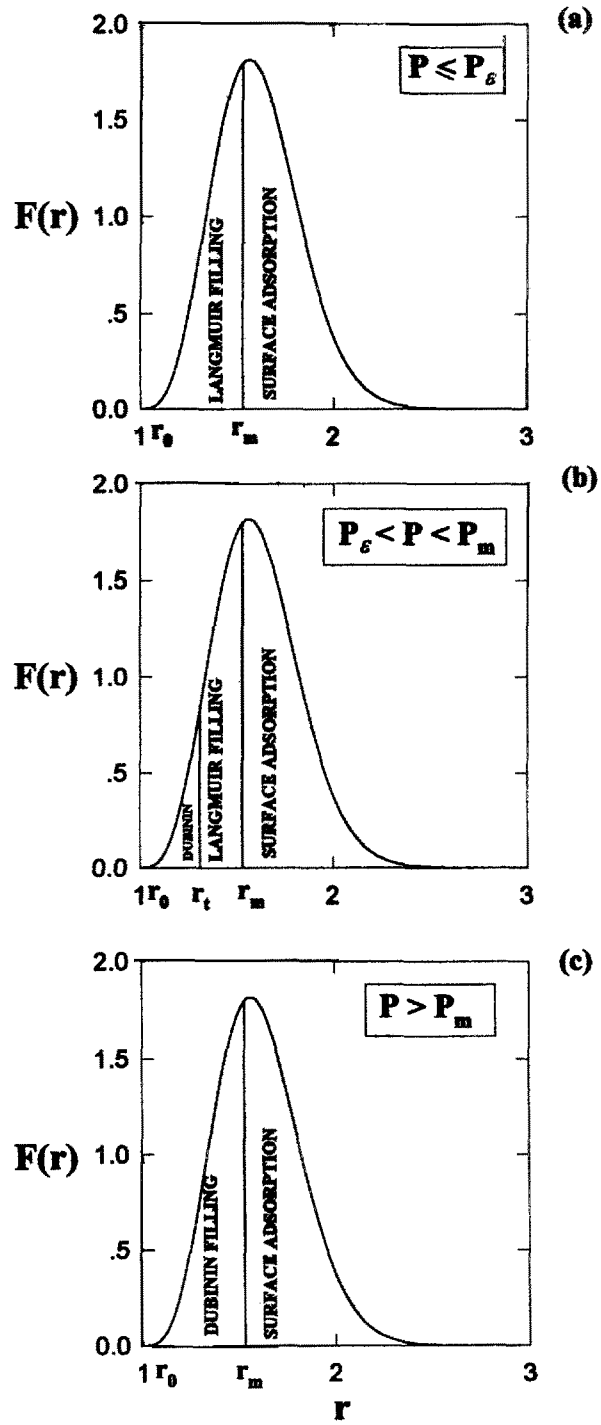

Fig. 1. Adsorption regime in different pore ranges and during different pressure ranges.

the pressure P_ε, the Dubinin pore filling mechanism is beginning to operate starting from the pore of size r_0, and for the gas pressure having values between P_ε and

P_m, the micropore range is divided into two, in each of which a different adsorption mechanism is operating. Let $r_t(P)$ be the threshold pore size corresponding to the gas pressure P, the Dubinin pore filling is operating in the range (r_0, r_t) and the Langmuir sorption is operating in the range (r_t, r_m) (Fig. 1b). As the gas phase pressure increases the threshold micropore size increases, that is more and more micropores are filled with sorbate molecules by the Dubinin mechanism, and when $P = P_m$, the threshold pore size reaches r_m, the demarcation between the micropore and the mesopore. When the gas pressure is greater than P_m, Dubinin pore filling is the only mechanism in the micropore (Fig. 1c). It is noted that in the mesopore range, the surface adsorption is the only mechanism operating throughout the whole pressure range, except when the pressure is reaching to the point (near vapor pressure) where capillary condensation starts to occur.

3.2 *The Threshold Pressure P_ε*

The lowest pressure that the Dubinin pore filling starts to occur in the micropore is the threshold pressure corresponding to the smallest pore size r_0. Since it is significant in understanding the onset of the pore filling mechanism, we investigate the behaviour of this pressure P_ε as a function of various parameters of the system, such as the exponent n in the Dubinin equation, T and r_0.

Figure 2 shows the variation of this threshold pressure P_ε with temperature and the exponent n is used as a parameter in the plot. The value of the smallest pore size is 1.01 nm. We see in this figure that as the temperature decreases, the threshold pressure also decreases, suggesting that the Dubinin pore filling mechanism starts to take effects earlier. This is expected because the vapor pressure is lower.

The exponent n is regarded as the parameter characterizing the heterogeneity of the solid, with larger value of n implying more homogeneous solid. Figure 2 shows that for a given temperature, the threshold pressure P_ε increases as the solid is becoming more homogeneous (i.e. larger n). This means that if the solid is heterogeneous, the onset of the Dubinin pore filling will occur sooner than the homogeneous solid. One could view that the surface roughness and the irregularities in the micropores would induce this onset of pore filling. The following table lists the ratio of the threshold pressure P_ε to the vapor pressure for various T and exponent n.

	n		
T (K)	2	2.2	2.3
303	0.155×10^{-4}	0.158×10^{-3}	0.345×10^{-3}
353	0.324×10^{-3}	0.175×10^{-2}	0.327×10^{-2}

Figure 3 shows the plots of the threshold pressure P_ε versus temperature with the smallest pore size r_0 as the parameter. The value of 2 was used for the Dubinin exponent. For a given temperature, the threshold pressure P_ε decreases with a decrease in r_0, which is entirely

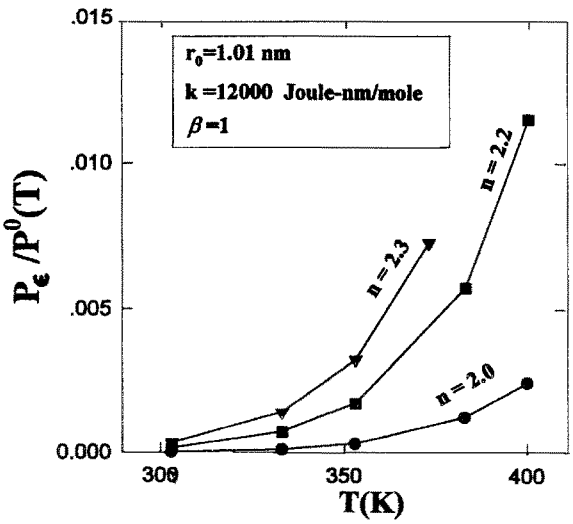

Fig. 2. Plot of minimum pressure for the onset of Dubinin isotherm versus temperature with Dubinin variable exponent as parameter.

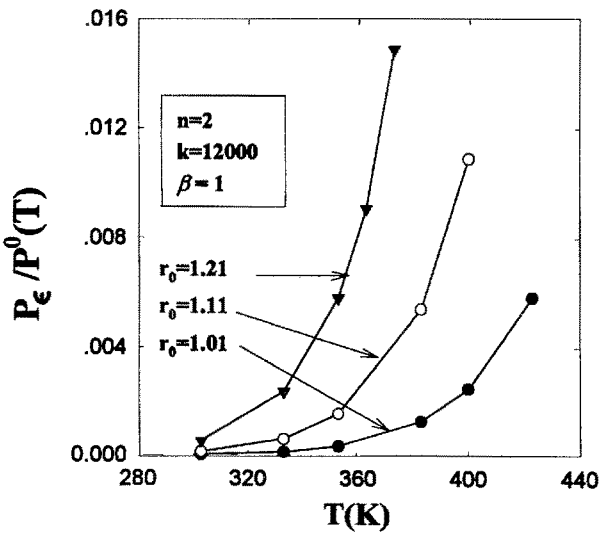

Fig. 3. Plot of minimum pressure for the onset of Dubinin isotherm versus temperature with the smallest micropore half width as parameter.

expected because the onset of the Dubinin pore filling mechanism would occur sooner in solids having smaller r_0. In heterogeneous solids having a broad micropore size distribution, it is then expected that the onset will occur at very low pressure. The following table lists some values of P_ε/P^0 as function of r_0 and temperature.

	r_0(nm)		
T (K)	1.01	1.11	1.21
303	0.155×10^{-4}	0.111×10^{-3}	0.524×10^{-3}
353	0.324×10^{-3}	0.154×10^{-2}	0.580×10^{-2}

3.3 *Demarcation Pore Size r_m, Affinity K_m and Threshold Pressure P_m*

While the smallest micropore size is intrinsic to the solid, the micropore size r_m, demarcating between micropore and mesopore, is a function of the system under consideration. In other words, it is a function of the adsorbate-adsorbent pairs (Shetna and Bhatia, 1994). Figure 4 shows the demarcation pore size as a function of temperature and the Dubinin exponent n. For a given adsorbent-adsorbate pairs, that is for a given n, the demarcation pore size decreases with an increase in temperature. This means that the range of the micropore is smaller at high temperature compared to that at lower temperature.

For a given temperature, the demarcation pore size r_m decreases with an increase in n (that is the solid is becoming more homogeneous), suggesting that the micropore range is smaller in homogeneous solids than in heterogeneous solids.

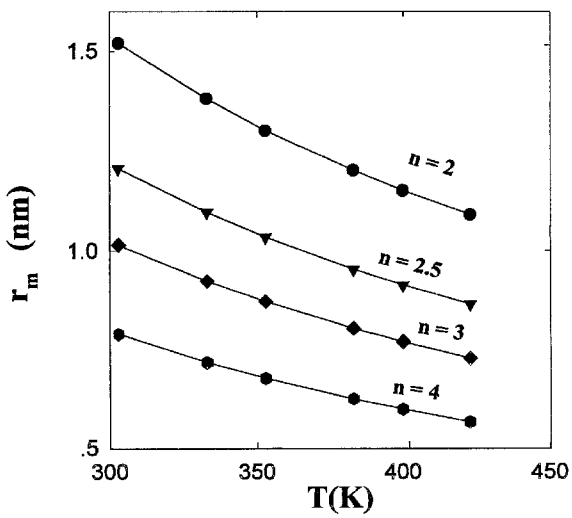

Fig. 4. Variation of maximum micropore half width with temperature, Dubinin variable exponent as parameter.

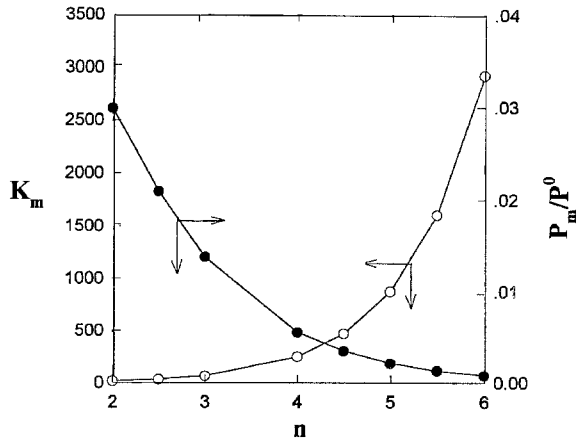

Fig. 5. Variation of Langmuir parameter and threshold pressure at maximum micropore half width with Dubinin variable exponent.

The following table shows values of the demarcation pore size (nm) for various values of n and temperatures:

	T (K)		
n	303	353	400
2.0	1.52	1.30	1.15
3.0	1.015	0.871	0.769

The Langmuir affinity and the threshold pressure corresponding to the demarcation pore size r_m are plotted in Fig. 5 as a function of the Dubinin exponent n. It is seen in this figure that the affinity K_m increases with a decrease in n (i.e., an increases in the extent of surface heterogeneity).

3.4 *Threshold Micropore Size r_t*

Figure 6 shows the plots of the threshold micropore size as a function of pressure. One plot is for a temperature of 353 K, and the other for 383 K. The lower limit of the threshold micropore size is the smallest accessible pore size of the solid, r_0. On the other hand, the upper limit of the threshold micropore size is system-specific, as we have discussed in the last section. For example, the upper limit of the threshold pore size (demarcation pore size) is 1.3 nm and 1.2 nm for 353 K and 383 K, respectively. The range of pressure in which the division of the micropore is effective in between P_ε and P_m. For a given system, the minimum threshold pressure P_ε is a function of T as we have discussed in Section 3.2, while the maximum threshold pressure

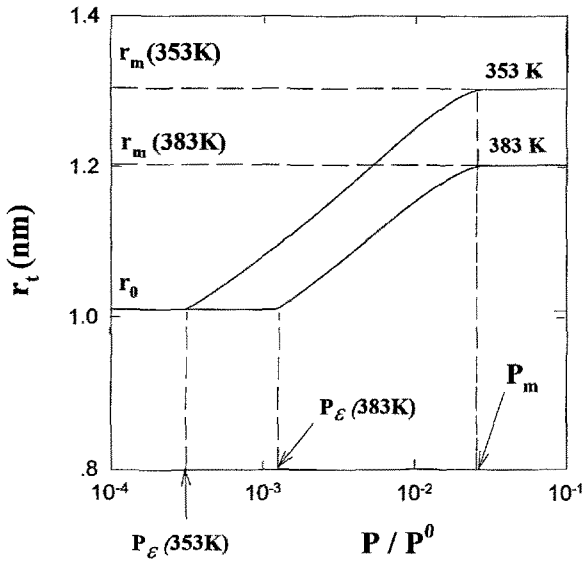

Fig. 6. Plot of threshold micropore half width versus pressure at different temperatures.

P_m is independent of T. The following table shows the range of the threshold pressure as a function of temperatures.

T (K)	333	353	383	400	423
P_ε/P^0	0.111×10^{-3}	0.324×10^{-3}	0.126×10^{-2}	0.247×10^{-2}	0.582×10^{-2}
P_m/P^0			0.0298		

3.5 *Overall Fractional Loading*

Having understood the behaviours of the threshold pressure and the threshold pore size, we now study the overall fractional loading and understand how each adsorption mechanism would contribute to the overall loading. Using the parameters listed in the table below, we simulate the overall fractional loading (Eq. 14) and the individual contributions of each adsorption mechanism, and the results are shown in Fig. 7.

T (K)	V_μ (cc/g)	v_M (cc/mol)	A(m^2/mol)	k(J.nm/mol)	r_0(nm)	r_m(nm)	σ	n	a	β
283	0.45	88.74	120×10^3	12000	1.01	1.61	0.218	2	1	1

The minimum and maximum threshold pressures for this set of parameters are $P_\varepsilon/P^0 = 0.297 \times 10^{-5}$ and $P_m/P^0 = 0.0298$, respectively. The minimum threshold pressure is very small, suggesting that over most

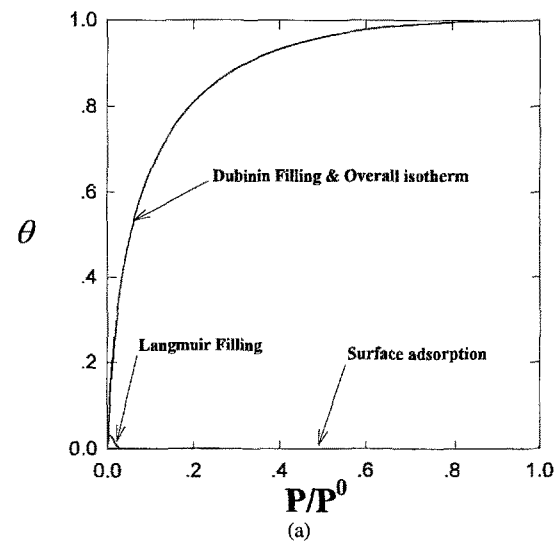

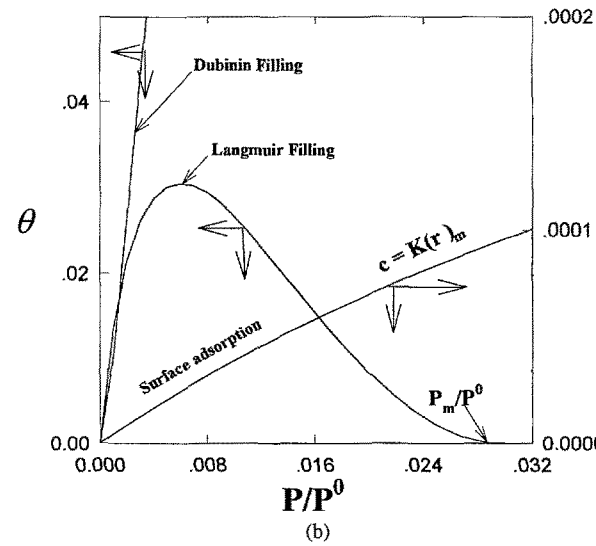

Fig. 7. Plot of overall amount adsorbed together with the individual contribution of Dubinin, Langmuir filling and surface adsorption versus pressure at 283° K. (a) Full scale. (b) Small scale.

range of the pressure the dominating mechanism in the micropore is the Dubinin pore filling (Fig. 7a). To show the contribution of the Langmuir sorption in micropore, Fig. 7b shows the behaviour at small pressure. We see that the Langmuir sorption increases with gas phase pressure, reaches its maximum value, decreases gradually and then ceases at pressure P_m. This behaviour for Langmuir sorption in micropore comes from the fact that it is only operative in the pressure range $0 < P < P_m$.

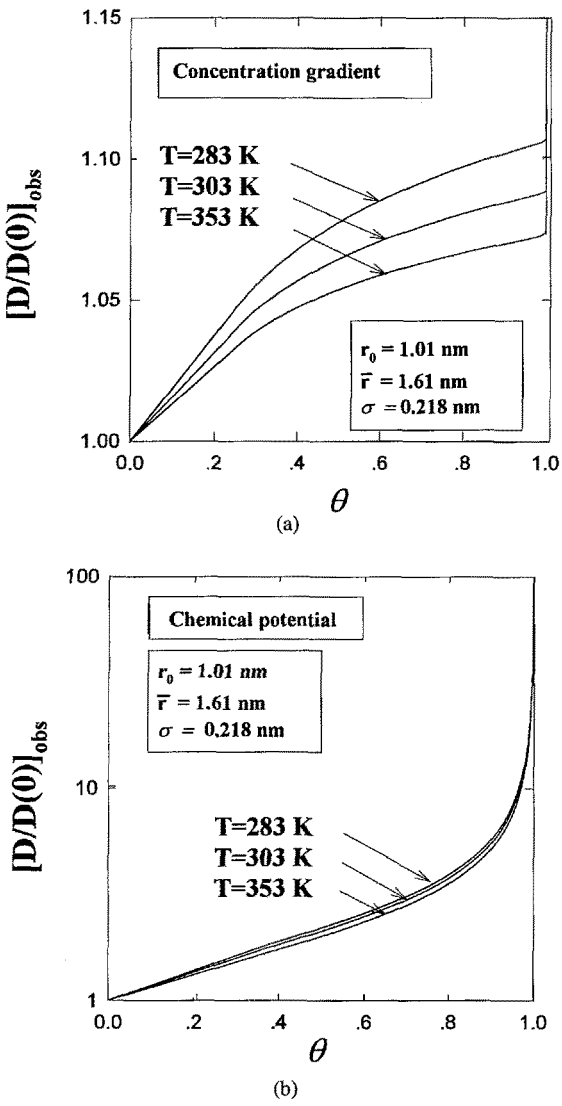

Fig. 8. Plot of relative observed surface diffusivity versus fractional loading with temperature as parameter. (a) Concentration gradient as the driving force. (b) Chemical potential as the driving force.

3.6 *Observed Surface Diffusivity*

3.6.1 Effect of Temperature Effect. In Fig. 8 we plotted the observed surface diffusivity versus the overall fractional loading for the cases of concentration gradient as the driving force (Fig. 8a) and chemical potential as the driving force (Fig. 8b). When the chemical potential gradient is the driving force, the observed surface diffusivity increases significantly with the overall fractional loading. Note the scale difference between Figs. (8a) and (8b). For a given fractional loading, the observed diffusivity decreases with an increase in temperature for both cases, although the percentage decrease is very small in the case of chemical potential gradient.

3.6.2 Effect of Smallest Pore Size r_0. The effect of the smallest micropore size r_0 on the observed surface diffusivity is shown in Fig. 9. For the case of concentration gradient as the driving force (Fig. 9a) solids with larger r_0 have lower relative observed surface diffusivity. This is explained as follows. First,

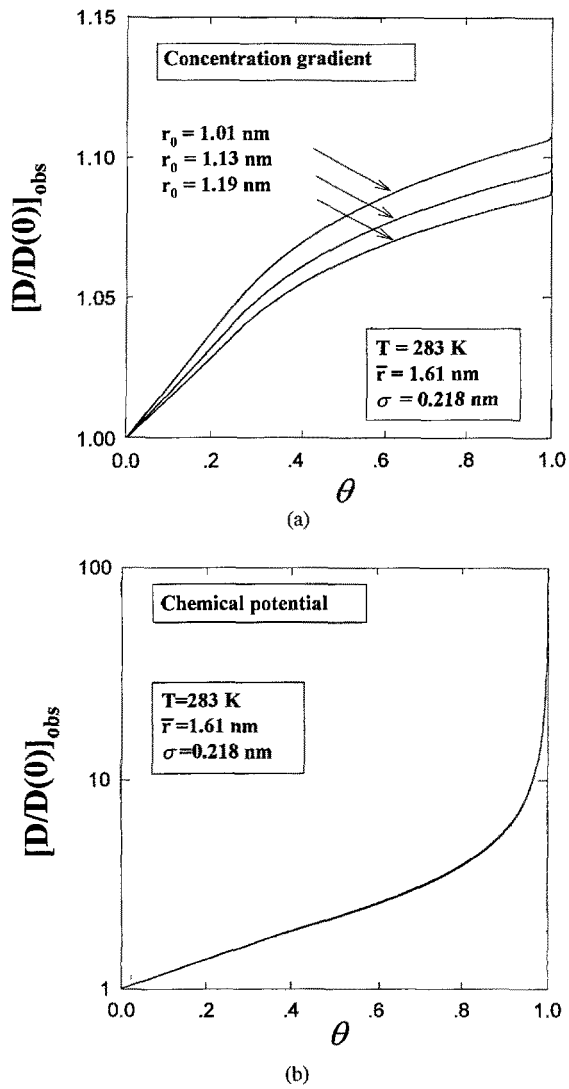

Fig. 9. Plot of relative observed surface diffusivity versus fractional loading for systems with the same mean pore half width and pore variance but with different minimum pore half width. (a) Concentration gradient as the driving force. (b) Chemical potential as the driving force.

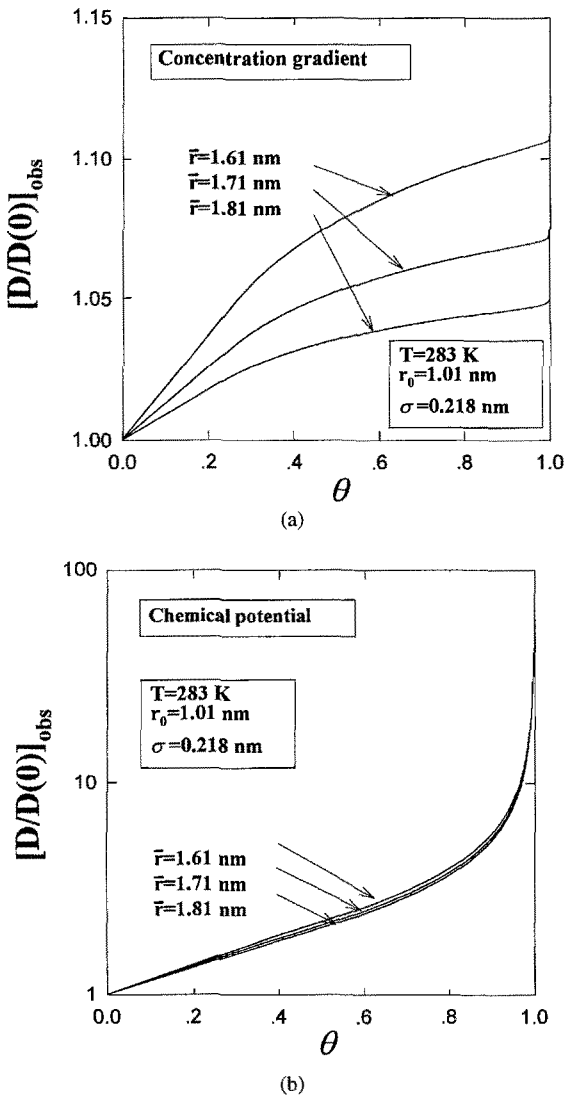

Fig. 10. Plot of relative observed surface diffusivity versus fractional loading for systems with the same minimum pore half width and pore variance but with different mean pore half width. (a) Concentration gradient as the driving force. (b) Chemical potential as the driving force.

note that the relative observed surface diffusivity is scaled with respect to the surface diffusivity at zero loading. At loadings very close to the zero loading, sorption occurs mainly in smallest pores and surface diffusion is due to those pores; hence the surface diffusivity at zero loading will reflect the low mobility in the smallest pores. Thus, solids with smaller r_0 will have lower values of the surface diffusivity at zero loading. Because of this lower value of $D(0)$, the rate of increase in the observed surface diffusivity will be higher in solids having smaller r_0, as we have seen in Fig. 9a. However, in the case of chemical potential driving force the effect of r_0 is negligible (Fig. 9b).

3.6.3 Effect of the Mean Pore Size and Pore Variance. Figure 10 show the effect of the mean pore size on the observed surface diffusivity. The dependence of the observed surface diffusivity on the mean pore size is similar to that on r_0. Keeping the mean pore size constant, the effect of the pore variance is shown in Fig. 11, where we noted that the dependence is stronger

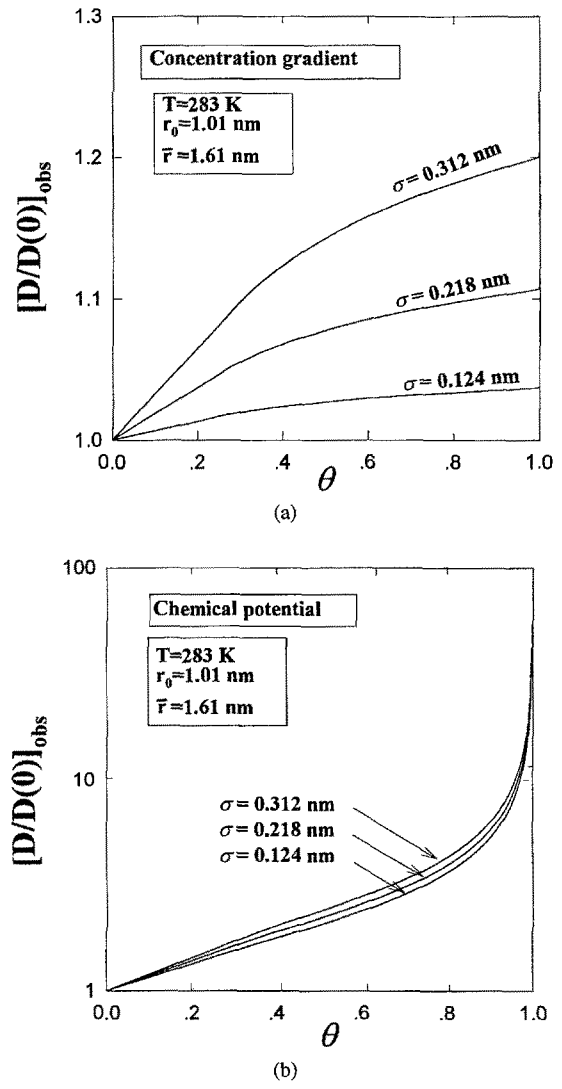

Fig. 11. Plot of relative observe driving forced surface diffusivity versus fractional loading for systems with the same minimum and mean ce.pore half width but with different pore variance. (a) Concentration gradient as the driving force. (b) Chemical potential as the driving force.

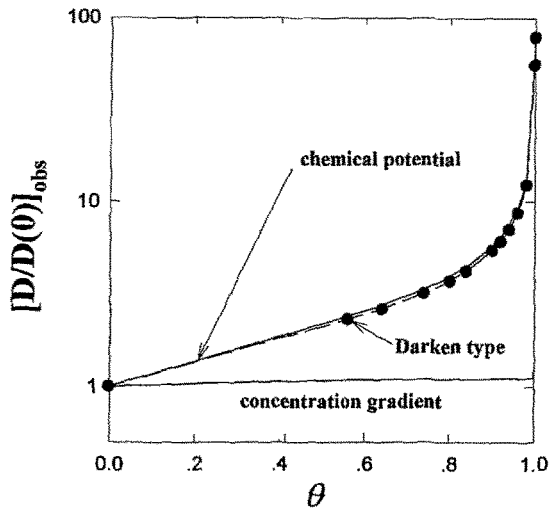

Fig. 12. Plot of relative surface diffusivity for the Darken-type case, the chemical potential and the concentration gradient driving force cases versus fractional loading.

when the pore size variance is changed, although the dependence is small in the case of chemical potential as driving force (Fig. 11b).

3.6.4 The Thermodynamic Correction Factor. In Fig. 12 we compared the relative observed surface diffusivity versus fractional loading for both chemical potential and concentration gradient driving force cases with the Darken-equation of surface diffusivity (Eq. 27). The chemical potential curve and the Darken type curve are almost superimposed on each other, suggesting that when the Darken relation is calculated, the thermodynamic correction factor, $\partial \ln P / \ln C$, completely contains the information on the micropore size distribution.

4 Conclusion

A hybrid isotherm was used in this study to investigate the effect of pore size distribution on the surface diffusivity in porous solids. This study demonstrates the concept of minimum pressure P_ε for the onset of Dubinin mechanism, and the upper limit of the micropore range r_m, which is dependent on the heterogeneity characteristics of solids, the energy characteristic of adsorbate as well as the temperature of the sorption system, meaning that the micropore range is system-specific. The Darken formula gives the relative surface diffusivity which is identical to the observed surface diffusivity derived from the local surface flux with chemical potential as the driving force, indicating that the thermodynamic correction factor in the Darken equation contains information about system heterogeneity.

Nomenclature

a	coefficient for surface diffusivity
A	adsorbate molecular area
c	affinity parameter of the surface adsorption isotherm
$C(P, T)$	concentration
C_{max}	maximum adsorbed concentration
D_{obs}	observed surface diffusivity
D_s	intrinsic surface diffusivity
D_{s0}	coefficient of intrinsic surface diffusivity
E_0	characteristic energy of Dubinin isotherm
$F(r)$	pore size distribution
J	local flux
J_{obs}	observed flux
k	empirical constant of Dubinin isotherm
K	Langmuir affinity parameter
K_m	Langmuir affinity parameter at maximum micropore half width
m	structural parameter defined in Eq. (13)
n	Dubinin variable exponent
q	structural parameter defined in Eq. (13)
Q	function of r and T defined in Eq. (4)
Q_m	function of n defined in Eq. (8)
P	pressure
P^0	vapour pressure
P_t	threshold pressure defined in Eq. (3)
P_0, P_L	pressure at two end of the slab
P_ε	minimum pressure for Dubinin isotherm
P_m	threshold pressure at maximum micropore half width
S_1, S_2	scaling factors defined in Eq. (15)
r	pore half width
r_0	smallest micropore half width
r_t	threshold micropore half width demarcates Dubinin and Langmuir mechanisms
r_m	maximum micropore half width
v_M	liquid molar volume of adsorbate
V	pore volume
R	gas constant
T	temperature
x	axial variable

Greek symbols

α	parameter defined in Eq. (A-7)
β	affinity factor of Dubinin isotherm
γ_L	constant defined in Eq. (A-7)
ε	small number
σ	pore variance
θ	non dimensional local isotherm
θ_D	non dimensional Dubinin isotherm
θ_L	non dimensional Langmuir isotherm
θ_S	non dimensional surface isotherm
θ_{obs}	non dimensional overall adsorption isotherm

Acknowledgment

This project is supported by the Australian Research Council.

Appendix

$$\langle\theta_D\rangle_1 = \varepsilon \int_{r_0}^{r_t(P_L)} 2S_1 \left(\frac{r}{\alpha}\right)^2 \gamma_L \exp\left[-\left(\frac{r}{\alpha}\right)^2 \gamma_L^2\right] \times F(r)dr \tag{A-1}$$

$$\langle\theta_L\rangle_1 = \varepsilon \int_{r_t(P_L)}^{r_m} S_1 \frac{\left(\frac{K}{P^0}\right)P_L}{\left[1+\left(\frac{K}{P^0}\right)P_L\right]^2} F(r)dr \tag{A-2}$$

$$\langle\theta_S\rangle_1 = \varepsilon \int_{r_m}^{\infty} S_2 \frac{\left(\frac{c}{P^0}\right)P_L}{\left[1+\left(\frac{c-1}{P^0}\right)P_L\right]^2} \frac{F(r)}{r}dr \tag{A-3}$$

$$\langle\theta_D\rangle_2 = \varepsilon \int_{r_0}^{r_t(P_L)} 2S_1 \left(\frac{r}{\alpha}\right)^2 \gamma_L \exp\left(-a\frac{\alpha}{r}\right) \times \exp\left[-\left(\frac{r}{\alpha}\right)^2 \gamma_L^2\right] F(r)dr \tag{A-4}$$

$$\langle\theta_L\rangle_2 = \varepsilon \int_{r_t(P_L)}^{r_m} S_1 \exp\left(-a\frac{\alpha}{r}\right) \times \frac{\left(\frac{K}{P^0}\right)P_L}{\left[1+\left(\frac{K}{P^0}\right)P_L\right]^2} F(r)dr \tag{A-5}$$

$$\langle\theta_S\rangle_2 = \varepsilon \int_{r_m}^{\infty} S_2 \exp\left(-a\frac{\alpha}{r}\right) \times \frac{\left(\frac{c}{P^0}\right)P_L}{\left[1+\left(\frac{c-1}{P^0}\right)P_L\right]^2} \frac{F(r)}{r}dr \tag{A-6}$$

where α and γ_L are

$$\alpha = \frac{\beta k}{RT}, \quad \gamma_L = \ln\left(\frac{P^0}{P_L}\right) \tag{A-7}$$

and a has been experimentally observed for many systems to lie between 1/3 and 1.

$$\langle\theta_D\rangle_3 = \varepsilon \int_{r_0}^{r_t(P_L)} \alpha S_1 \exp\left(-a\frac{\alpha}{r}\right)\left(\frac{1}{r}\right) \times \left[\left(\frac{r}{\alpha}\right) - \left(\frac{r}{\alpha}\right)^3 \gamma_L^2 + \sum_{i=1}^{N} \frac{(-1)^{(i+1)}}{(i+1)!} \times \left(\frac{r}{\alpha}\right)^{(2.i+3)} \gamma_L^{2.i+2}\right] F(r)dr \tag{A-8}$$

$$\langle\theta_L\rangle_3 = \varepsilon \int_{r_t(P_L)}^{r_m} S_1 \exp\left(-a\frac{\alpha}{r}\right) \times \frac{\left(\frac{K(r)}{P^0}\right)P_L}{1+\left(\frac{K(r)}{P^0}\right)P_L} F(r)dr \tag{A-9}$$

$$\langle\theta_S\rangle_3 = \varepsilon \int_{r_m}^{\infty} S_2 \exp\left(-a\frac{\alpha}{r}\right) \times \frac{\left(\frac{c}{P^0}\right)P_L}{1+\left(\frac{c-1}{P^0}\right)P_L} \frac{F(r)}{r}dr \tag{A-10}$$

References

Bhatia, S.K. and H.K. Shethna, "A modified pore filling isotherm with application to determination of pore size distribution," *Langmuir*, **10**, 3230–3243 (1994).

Do, D.D. and H.D. Do, "Effect of micropore size distribution on the surface diffusivity in microporous solids," *Chem. Eng. Sci.*, **48**, (14), 2625–2642 (1993).

Dubinin, M.M. and V.A. Astakhov, "Description of adsorption equilibrium of vapors in zeolites over a wide range of temperature and pressure," *Adv. Chem.*, **102**, 69 (1971).

Dubinin, M.M. and L.V. Radushkevich, "The equation of the characteristic curve of activated charcoal," *Dokl. Akad. Nauk SSSR*, **55**, 327 (1947).

Gregg, G.R. and K.S.W. Sing, *Adsorption, Surface Area and Porosity*, Academic Press, New York, 1982.

Jaroniec, M. and R. Madey, *Physical Adsorption on Heterogeneous Solids*, Elsevier, Amsterdam, 1988.

Rudzinski, W. and D.H. Everett, *Adsorption of gases on heterogeneous surfaces*, Academic Press, London, 1992.

Shethna, H.K. and S.K. Bhatia, "Interpretation of adsorption isotherms at above-critical temperatures using a modified micropore filling model," *Langmuir*, **10**, 870–876 (1994).